AIAA JOURNAL
Vol. 42, No. 12, December 2004

Analysis of Unsteadiness in Afterbody Transonic Flows

D. Deprés* and P. Reijasse†
ONERA, 92190 Meudon, France
and
J. P. Dussauge‡
Institut Universitaire des Systèmes Techniques et Industriels, 13003 Marseille, France

Separated flows behind afterbodies in the high subsonic regime are investigated experimentally. Measurements of mean and unsteady wall pressure have been performed in a transonic wind tunnel on axisymmetric configurations with a propulsive jet. It is found that the distance between the base plane and the nozzle exit section, namely, the rear-body extension, is a determining parameter. For a long enough rear-body extension, the separated flow reattaches at the end of the external nozzle wall. The spectra in the reattachment region exhibit a weakly defined maximum, which is associated with the shear layer vortices impinging the downstream surface. For a short rear-body extension, the reattachment on the downstream nozzle wall is not possible. The spectra in the whole region exhibit a well-defined periodicity that corresponds to the formation of large-scale structures in the wake, as observed for bluff bodies. This is confirmed by a two-point correlation analysis of the turbulent signals, which shows that the flow is dominated by a highly coherent antisymmetric mode at the vortex shedding frequency.

Nomenclature

C	=	complex coherence function, $C_r + iC_i$
C_p	=	wall static pressure coefficient, $(p - p_\infty)/q_\infty$
$C_{p\,\mathrm{rms}}$	=	unsteady wall pressure coefficient, $p_{\mathrm{rms}}/q_\infty$
D	=	forebody diameter (100 mm)
d	=	rear-body diameter (40 mm)
f	=	frequency
G	=	power spectral density
L	=	rear-body extension, distance from the base
M	=	Mach number
p	=	local static pressure
p_{rms}	=	root-mean square of the pressure fluctuation
p_{st}	=	jet stagnation pressure
q	=	dynamic pressure, $0.5\gamma pM^2$
S_{12}	=	cross-spectral density
Sr_l	=	Strouhal number based on length $l = L$ or D, fl/U_∞
U	=	streamwise velocity
X	=	streamwise distance (0 in the base plane)
γ	=	modulus of the coherence function, $\lvert C\rvert$
δ	=	boundary-layer thickness
Φ	=	coherence phase angle, deg
φ	=	azimuthal position, deg

Subscripts

r	=	reattachment
∞	=	freestream conditions

Presented as Paper 2003-3469 at the AIAA 33rd Fluid Dynamics Conference, Orlando, FL, 23–26 June 2003; received 11 December 2003; revision received 14 May 2004; accepted for publication 31 May 2004.

*Ph.D. Student, Fundamental and Experimental Aerodynamics Department, 8 rue des Vertugadins.

†Research Scientist, Fundamental and Experimental Aerodynamics Department, 8 rue des Vertugadins.

‡Directeur de Recherche, Unité Mixte de Recherche, Centre National de la Recherche Scientifique–Université de Provence No. 6595, 12 avenue Général Lederc.

Introduction

THE afterbody flow around a launcher is characterized by a large separation because of an abrupt change in the geometry. The first consequence of this base geometry is the creation of a specific drag due to a low-pressure level in the separated region. Second, the base region is submitted to dynamic loads generated by aerodynamic excitation, especially during the high dynamic pressure phase of flight. More precisely, this buffet is induced by the unsteadiness of the separated flow, which generates strong low-frequency wall-pressure fluctuations. These oscillations can excite a response of the structural modes called buffeting. With the constant need of improving the aerodynamic performances of launch vehicles, the design of afterbodies requires knowledge of wall-pressure characteristics and of the unsteady flow mechanisms involved in the buffeting phenomenon.

The base pressure properties of blunt axisymmetric bodies have been studied experimentally by Eldred,[1] Mabey,[2] and Merz[3] for compressible subsonic flows. These investigations deal with the most simple rear geometry of revolution. Experimental results obtained on more complex axisymmetric afterbodies have shown that the wall pressure is highly dependent on the geometry and the presence of a propulsive jet, for instance, as shown in the compilation made by Délery and Sirieix.[4] Indeed, mainly two different kinds of base flow separation can be considered: whether a downstream reattachment of the shear layer on a solid surface does occur or does not.

In the case of the blunt-based body, the flow does not reattach on a downstream surface and is characterized by a mutual interaction of the separating shear layers, which results in the formation of large-scale vortices in the wake. The flow organization must be similar to that behind bluff bodies such as a sphere[5] or a circular disk,[6,7] which have been studied both at moderate Reynolds and low Mach numbers. It has been shown that the wake is dominated by a vortex shedding process possibly organized in a helical structure randomly oriented in the azimuthal direction.[5,6] These large-scale coherent structures are associated with an antiphase relationship of the velocity or pressure fluctuations between diametrically opposed positions across the wake. Strouhal numbers of 0.135 and approximately 0.2 have been reported for the disk and the sphere, respectively (Reynolds number dependent value). Unsteady vortex shedding in the sphere wake has been observed[7,8] for Reynolds numbers in the range from 400 to 3.7×10^5, where the boundary layer at separation is laminar. Boundary-layer transition at the critical Reynolds number 3.7×10^5 was associated with a drastic change in the wake flow regime, which became basically steady but with streamline organized non-axisymmetrically. However, in the case

of the blunt-based body,[9] a vortex shedding process was shown to exist in the wake for high Reynolds numbers at high subsonic speeds. Indeed, a periodicity was found in the streamwise velocity fluctuations that was related to the wake oscillations. The corresponding Strouhal number in the wake was 0.2, which should be compared to the 0.246 value reported by Calvert.[10] Nevertheless, these large-scale structures did not seem to induce any particular wall-pressure fluctuations on the base.

Let us now consider more complex afterbody shapes characterized by an interaction of the separated shear layer with a downstream surface through the reattachment process. The review of Mabey[11] on wall-pressure fluctuations in recirculating regions, which covers a wide range of separating and reattaching flows, has shown that a good scaling parameter is the separation bubble length X_r. In the reattachment zone, the main flow unsteadiness is characterized by a Strouhal number $fX_r/U_\infty \approx 0.6$ associated with a weakly pronounced maximum in the wall-pressure spectra. In their rearward-facing step study, Driver et al.[12] showed that this unsteadiness could be related to the vortex rollup and pairing process as seen in free shear layers.

This paper presents an investigation of wall-pressure characteristics in the high subsonic regime for generic axisymmetric configurations representative of a launch vehicle afterbody. The main goal is to determine the major features of the mean flow structure and the predominant unsteady aerodynamic mechanisms involved in the generating process of wall-pressure fluctuations. Several configurations are considered. They range from the simple blunt-based body, which should be seen as a reference case, to more realistic geometries equivalent to an axisymmetric rearward-facing step of finite downstream extension and equipped with a nozzle. The choice of such afterbody configurations allows two parameters to be tested, the downstream extension of the axisymmetric step (herein referred to as the rear-body) and the influence of a supersonic propulsive jet on the external subsonic flow. The two categories of separated flows, with and without solid reattachment, should be obtained, depending on the rear-body extension compared to the reattachment distance.

Experiment

A series of tests were carried out at the Fundamental and Experimental Aerodynamics Department in the transonic S3Ch continuous wind tunnel whose test cross section is a square of 760×800 mm^2 area. The tunnel works with atmospheric air, and a heat exchanger in the settling chamber maintains a constant stagnation temperature during the tests. The freestream turbulence have been measured previously and was estimated to be 0.15%. Four model configurations were tested (Fig. 1). The first one was a cylindrical simple base (forebody diameter $D = 2R = 100$ mm). This geometry was chosen because it was the simplest one and it had already been investigated by several authors. From this configuration, a truncated ideal nozzle with a throat diameter of 12.93 mm was added at the base center. The exit nozzle diameter was 33 mm, and the Mach number at the lip was 3. The external nozzle surface was a cylindrical body of diameter $d = 40$ mm. The exit section was first located in the base area plane $X = 0$. Then, the nozzle was shifted downstream at a distance L from the base. Two extensions of the cylindrical rear-body were investigated corresponding to $L/D = 0.6$ and 1.2. The test models were mounted at the end of a cylindrical forebody fixed in the wind-tunnel settling chamber. The nozzle was supplied through this forebody by a compressed air system with a maximum stagnation pressure of about 40 bar.

About 80 pressure taps were mounted on the cylindrical forebody (before the base corner), the base area, and the rear-body region, both in the streamwise and azimuthal directions. The wall static pressures were measured using PM131-Statham transducers, whereas XCQ-062-15A Kulite sensors were chosen to record simultaneously the fluctuating component at a sampling rate of 10,240 Hz. This allowed good resolution of the fluctuations regarding the low frequencies involved in the separated region. Because of the curvature of the surface, it was difficult for the unsteady transducers to be mounted flush with the wall. They were housed in a cavity of small volume.

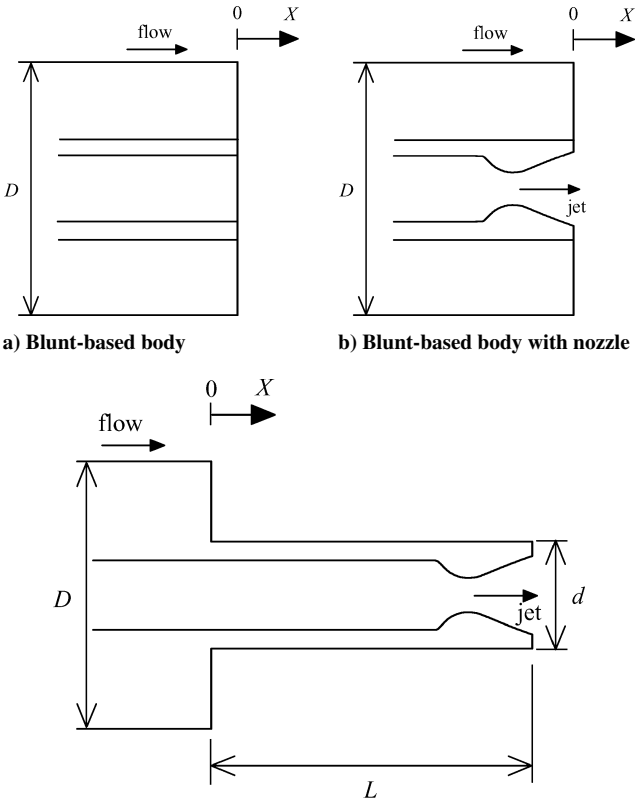

a) Blunt-based body **b) Blunt-based body with nozzle**

c) Nozzle exit section downstream of base, $L/D = 0.6$ and 1.2

Fig. 1 Schematic of axisymmetric afterbody models.

This induced a cutoff frequency of about 18 kHz that was much greater than the frequencies under consideration in this study.

To evaluate measurement uncertainties, a statistical approach was used based on a series of repeated independent experiments. In this way, all of the potential sources of error in the determination of the quantities are included, such as instrumentation noise or variations in the inflow conditions. The estimated uncertainties were typically 2 and 5% for the steady and unsteady pressure coefficients, respectively.

The different afterbody models were tested at zero incidence for three different freestream Mach numbers, 0.6, 0.7, and 0.85. The incoming flow was checked to be axisymmetric by using surface flow visualization and measuring the boundary-layer profile in each quadrant of the forebody. The initial external boundary layer, which was growing on the upstream cylindrical sting over a distance of about $10D$ before reaching the base corner, was fully turbulent. The thickness δ was measured using a pitot rake at $X/D = -2.45$, and the ratio δ/D was found to be approximately 0.20 for the three Mach numbers. The Reynolds number based on the forebody diameter D was about 1.20×10^6. The three model configurations equipped with a nozzle were first tested without jets as a reference. In this case, an airtight stopper was used to fill the nozzle exit to avoid cavity effects. Then, three internal flow regimes were considered through the nozzle pressure ratio (NPR) $= p_{st}/p_\infty$: jet at adaptation (NPR ≈ 33), overexpanded jet without separation (NPR ≈ 12.5), and overexpanded jet with separation (NPR ≈ 8.4).

Results and Discussion

No particular effect of freestream Mach number was observed in the measurements. Therefore, unless otherwise mentioned, the results are discussed for the $M_\infty = 0.85$ case.

Mean and Fluctuating Pressure Distributions

Reference Case: Blunt-Based Body

Figures 2 and 3 show that the static pressure is approximately constant over the blunt surface with a value lower than p_∞, that is, $C_p < 0$. The negative value of the pressure coefficient before

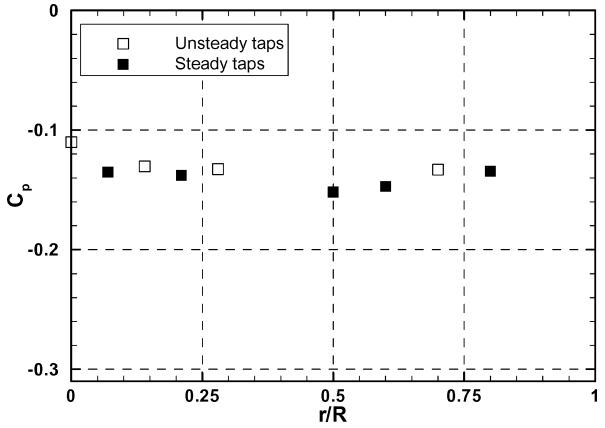

Fig. 2 Radial distribution of static base pressure for the blunt-based body, $\varphi = 0$ deg.

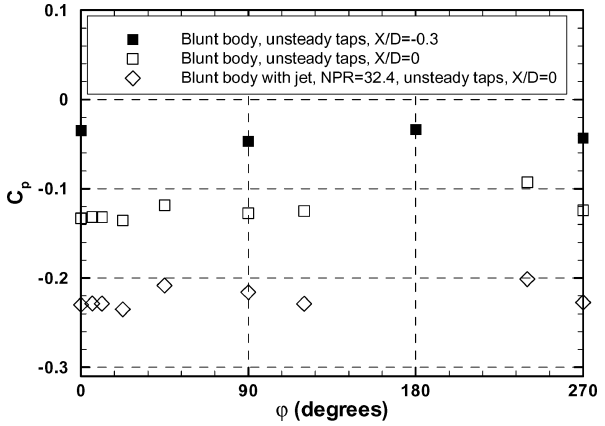

Fig. 3 Azimuthal distributions of static base pressure on the forebody, $X/D = -0.3$, and on the base, $X/D = 0$ and $r/R = 0.7$.

separation at $X/D = -0.3$ (Fig. 3) shows the upstream influence of the recirculation region on the attached boundary layer. The inflow is accelerated to match the base pressure in the $X = 0$ plane. The experimental data on the base area exhibit a small scatter in the azimuthal direction around a mean value $C_p = -0.124$. Merz[3] has reported a slightly higher constant value of $C_p = -0.11$ on a blunt-based body that was also mounted on an upstream sting. The pressure coefficient C_p measured in the present experiment is in good agreement with the commonly determined value for subsonic base flows[4] ($M_\infty \leq 0.85$), that is, $C_p \approx -0.125$. The measurements have been checked to be well reproducible inasmuch as at least two independent pressure acquisitions have been performed for each configuration. Hence, it is likely that these azimuthal pressure variations are due to some irregularities of the body shape or to the inflow in the test section of the wind tunnel. Moreover, the same azimuthal evolution of the static pressure is obtained for the other configurations, although with a different mean value, as shown in Fig. 3 for the blunt-based body with jet.

The rms distribution of the pressure fluctuations in the radial direction, together with Eldred's[1] and Mabey's[2] results, is plotted in Fig. 4 using the $C_{p\,\mathrm{rms}}$ coefficient. In the present measurements, the rms pressure level is higher at the base center with $C_{p\,\mathrm{rms}} \approx 0.027$ and decreases steadily as r/R increases to reach $C_{p\,\mathrm{rms}} \approx 0.014$ in the outer base region. This distribution is not in agreement with Eldred's[1] results, where the opposite behavior is observed. In Mabey's[2] experiment, the $C_{p\,\mathrm{rms}}$ levels are almost identical at $r/R = 0.3$ and 0.65. These apparent discrepancies can be partly explained with the azimuthal $C_{p\,\mathrm{rms}}$ distribution in Fig. 5, which is far from being homogeneous, suggesting a non-axisymmetric unsteady flow feature. In the present experiment, the base area of the blunt body can be divided into two regions, a first one with low rms values and another larger one with stronger pressure fluctuations. Hence, the radial $C_{p\,\mathrm{rms}}$ evolution on the base area depends on the

Table 1 Average azimuthal values[a] of C_p and $C_{p\,\mathrm{rms}}$ pressure coefficients at $r/R = 0.7$

	NPR			
Coefficient	32.4	12.4	8.3	No jet
$\langle C_p \rangle$	−0.223	−0.187	−0.179	−0.124
$\langle C_{p\,\mathrm{rms}} \rangle$	0.0175	0.0137	0.0130	0.0184

[a]Blunt body with and without jet.

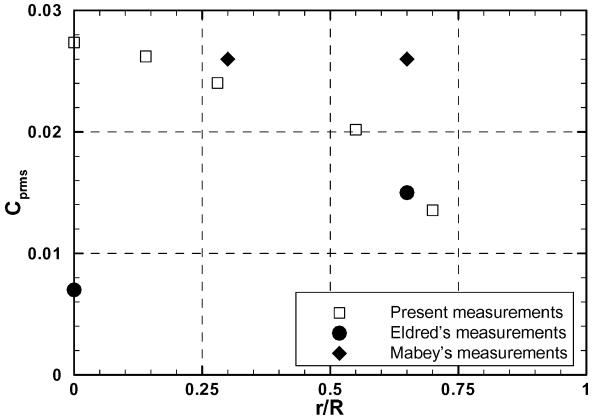

Fig. 4 Radial distributions of rms base pressure fluctuations, $\varphi = 0$ deg.

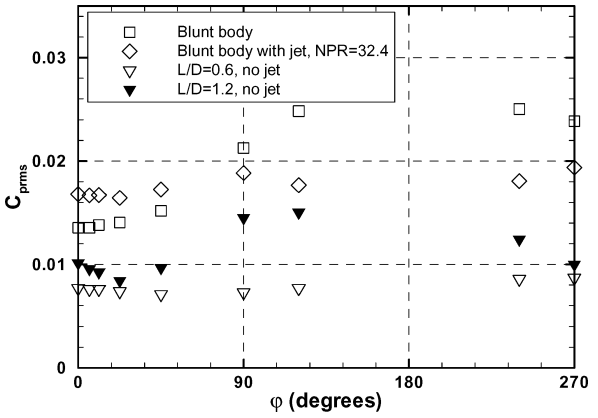

Fig. 5 Azimuthal distributions of rms base pressure fluctuations, $r/R = 0.7$.

azimuthal position of the pressure taps. For instance, at $\varphi = 240$ deg, $C_{p\,\mathrm{rms}} \approx 0.025$, which is not very far from the value at the center ($C_{p\,\mathrm{rms}} \approx 0.027$; Fig. 4). The other results shown in Fig. 5 show that the azimuthal $C_{p\,\mathrm{rms}}$ distributions are more or less uniform for the models with rear-body. This point suggests that the nonaxisymmetric unsteady flow feature of the blunt-based body is inherent to that configuration. In particular, it is not directly related to some irregularities in the incoming flow or to the model geometry.

Effect of Supersonic Jet

The supersonic jet directly interacts with the external recirculation region and strongly modifies the flow topology of the earlier afterbody configuration. As can be seen in Fig. 3 and Table 1 for the blunt-based body with jet, the wall pressure is noticeably decreased compared to the no-jet case. This behavior is known to be produced by the suction effect of the jet shear layer, which tends to empty the external recirculation region. The reduction of this effect when the NPR is decreased can be explained by the smallest size of the overexpanded jet radius, which induces a smaller circumferential surface of the jet shear layer.

Compared to the simple blunt-based body situation, the rms base pressure is not higher with a jet, but the external flow is obviously more axisymmetric, as shown in Fig. 5. The jet probably stabilizes the whole near-wake flow. As shown in Table 1, the $C_{p\,\mathrm{rms}}$ level

depends on the NPR, and the highest value is obtained at adaptation. Notice that an internal separation of the jet induces strong wall-pressure fluctuations inside the nozzle as demonstrated by previous studies.[13,14] These have been checked in the present experiments using the unsteady transducers mounted in the nozzle wall just upstream of the lip. Hence, the present results show that the jet separation (NPR = 8.3) does not produce additional fluctuations of the external base pressure.

The turbulent pressure signals in Fig. 6 appear to be highly random and broad-band. In the no-jet case, a low-frequency oscillation at $\varphi = 240$ deg is clearly visible, which explains a part of the difference in the rms value with the $\varphi = 0$ deg position. When the jet is running, this component is attenuated and brief occurrences of positive high-pressure fluctuations are observed. These oscillations may be the signature of the jet noise generated after the nozzle exhaust.

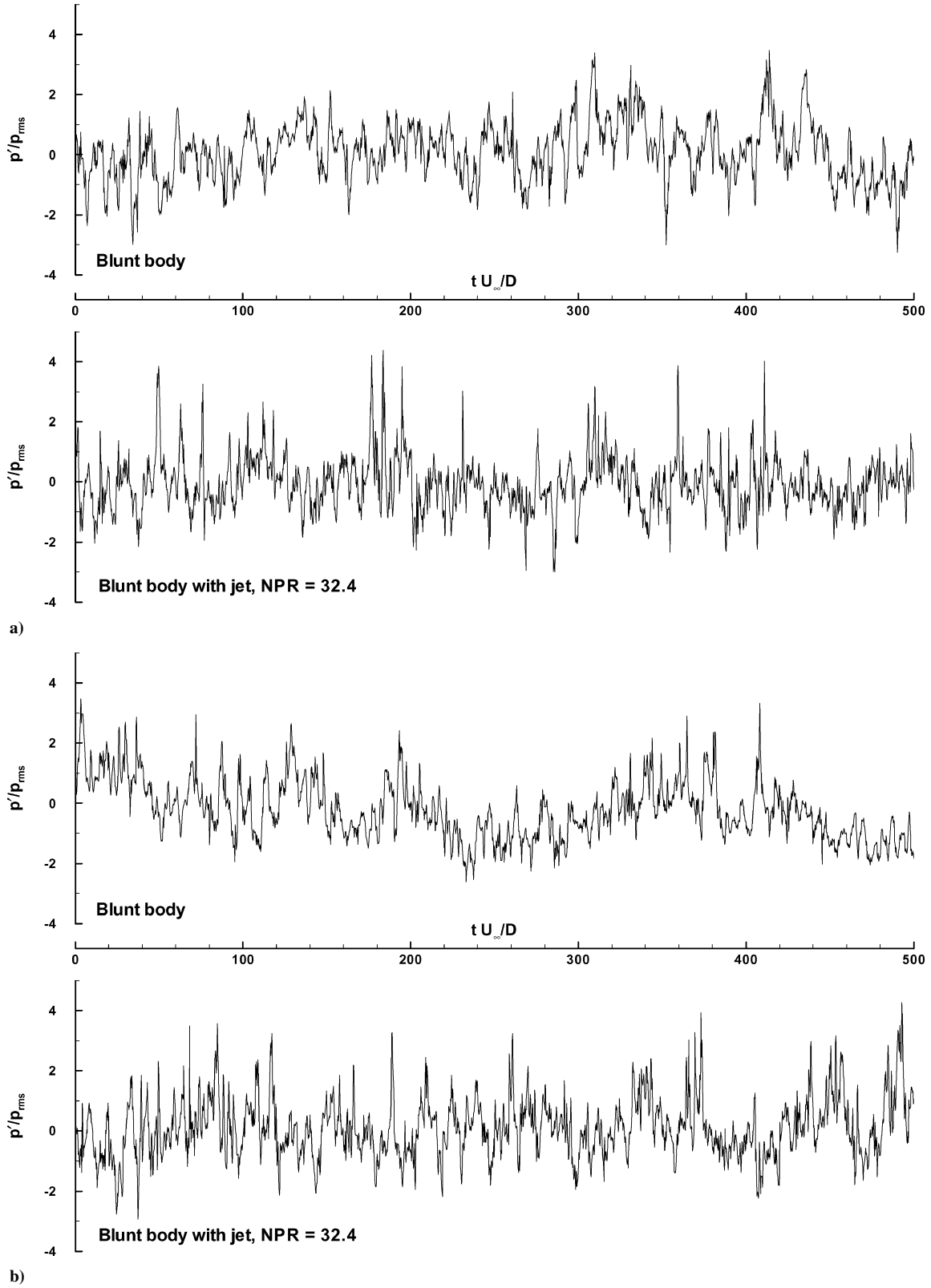

Fig. 6 Sample time series of base pressure fluctuations for $r/R = 0.7$ at $\varphi =$ a) 0 and b) 240 deg.

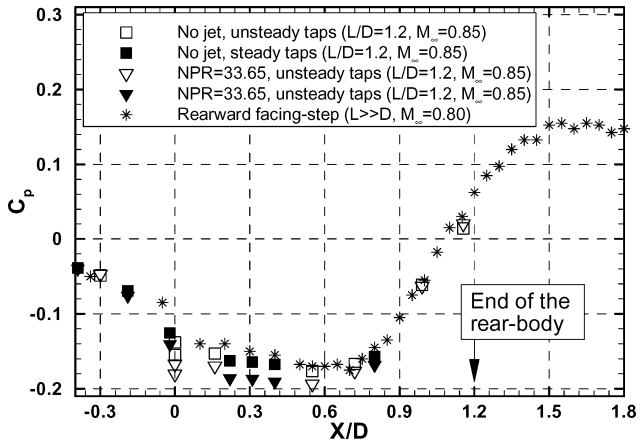

Fig. 7 Streamwise distributions of static pressure in the present tests, $L/D = 1.2$ and $M_\infty = 0.85$, and in a previous investigation,[15] $L/D >> 1$ and $M_\infty = 0.80$.

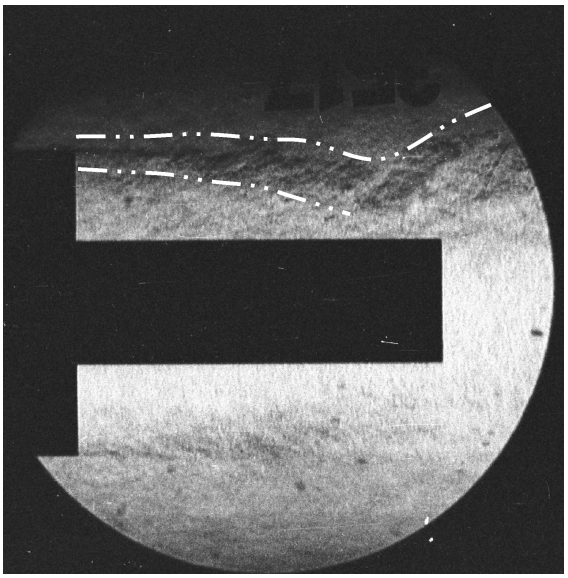

Fig. 8 Instantaneous schlieren photograph in the $L/D = 1.2$ case without jet at $M_\infty = 0.7$.

Effect of Rear-Body with No Jet

The effect of the ratio L/D corresponding to configurations with a protruding rear-body placed downstream of the base is now investigated. In these situations, the separated shear layer that starts developing at $X/D = 0$ can interact with the rear-body in a manner that depends on the geometric parameter L/D, whether a solid reattachment does occur or does not.

In the $L/D = 1.2$ case, Fig. 7 shows a small decrease of the wall pressure in the separated region up to $X/D \approx 0.5$ ($C_p \approx -0.17$). It is followed by a strong recompression, which indicates the beginning of a reattachment process on the rear-body surface. The maximum pressure is reached at the end of the rear-body and is slightly higher than p_∞. Hence, although the exact flow topology is unknown, it can be inferred that the shear layer reattaches at the end of the protruding cylinder ($X_r \approx L$). This is confirmed by the instantaneous schlieren photograph shown in Fig. 8. The separated shear layer starts curving at the middle of the rear-body and then impinges the wall. Figure 7 also shows the pressure measurements obtained from previous experiments[15] performed at $M_\infty = 0.8$ in the same wind tunnel on an axisymmetric afterbody equipped with a very long cylindrical rear-body ($L/D = 9$). The values of the diameters D and d were the same as in the present study. This configuration corresponds to the axisymmetric rearward-facing step in the literature. In this case, the reattachment length was estimated to be approximately

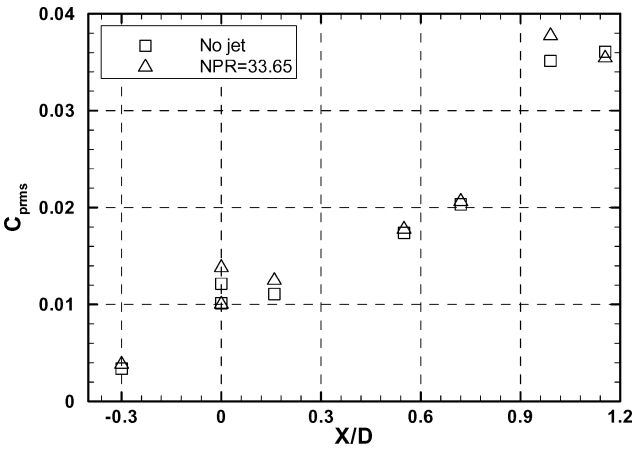

Fig. 9 Streamwise distributions of the rms pressure fluctuations in $L/D = 1.2$ case.

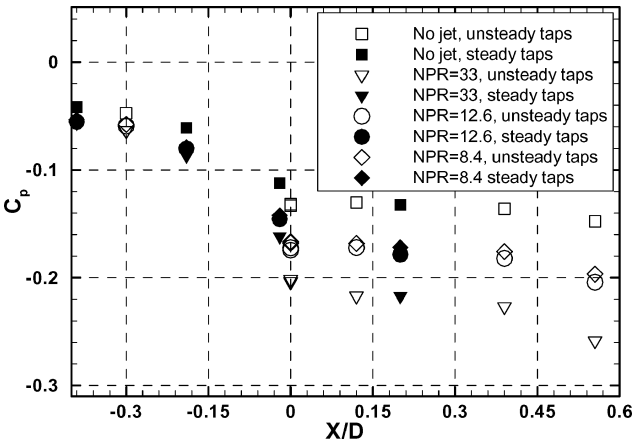

Fig. 10 Streamwise distributions of static pressure in $L/D = 0.6$ case.

$X_r/D = 1.3$ using surface flow visualization and reattachment was located just upstream of the maximum pressure position. With regard to the pressure fluctuations, the $C_{p\,\mathrm{rms}}$ level (Fig. 9) increases steadily from the base in the streamwise direction with a growth rate more pronounced for $0.6 < X/D < 1$. This behavior in the recirculation region has already been described by Mabey.[11] Mabey has shown that the maximum rms of the wall-pressure fluctuations is reached just upstream of the mean shear layer reattachment position. In the present situation, a plateau seems to be reached near the end of the rear-body at $X/D \approx 1$ ($C_{p\,\mathrm{rms}} \approx 0.035$). This behavior should be seen as another sign of a solid reattachment at the end of the rear-body.

When $L/D = 0.6$, the wall-pressure distribution on the rear-body (Fig. 10, square symbols) is characterized by a slow decay as the streamwise position increases. The average value of the mean pressure coefficient on the rear-body, $C_p \approx -0.14$, is, however, slightly higher than in the $L/D = 1.2$ case for $X/D \leq 0.6$, where $C_p \approx -0.17$. Finally, there is no recompression process at the end of the rear-body, which is too short for a solid reattachment to occur. Hence, the flow organization should be dominated by the formation of discrete vortices in the near wake, as for the blunt-based configuration.[9] The $C_{p\,\mathrm{rms}}$ streamwise distribution shown in Fig. 11 is similar to that obtained with $L/D = 1.2$ for $X/D \leq 0.6$. However, here the maximum of the pressure fluctuations is reached at the end of the rear-body and $C_{p\,\mathrm{rms}}$ is only 0.015.

Effect of Supersonic Jet with Rear-Body

The jet influence in the preceding configurations is now investigated through the streamwise wall-pressure distributions. In the $L/D = 1.2$ case, both the mean and fluctuating pressure (Figs. 7 and 9) are weakly modified by the presence of the jet. This result

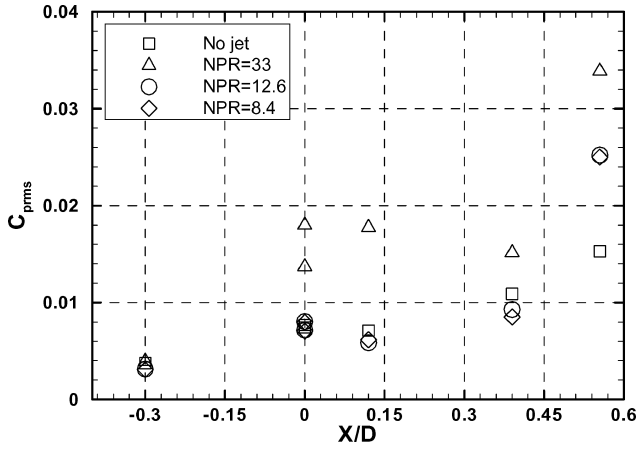

Fig. 11 Streamwise distributions of rms pressure fluctuations in the *L/D* = 0.6 case.

is consistent with the solid reattachment of the external flow on the rear-body surface because, in this case, the jet is located farther downstream and does not directly interact with the subsonic recirculation region.

When the rear-body extension is reduced to $L/D = 0.6$, the situation changes drastically. For a given NPR, the static pressure all along the protruding surface (Fig. 10) decreases an approximately constant value compared to the no-jet situation. This strong depression in the recirculation region, which is due to the jet suction effect, influences the attached boundary layer up to $X/D = -0.4$. The decrease of the static pressure in the separated region is weaker for an overexpanded jet, and the situation approaches the no-jet case. This indicates a reduction of the jet influence. Concerning the rms values in Fig. 11, the highest levels by far are obtained for the jet at adaptation. With comparison to the no-jet situation, the $C_{p\,\mathrm{rms}}$ coefficient strongly increases in the base region and at the end of the rear-body, where it is more than twice as high. For the two other NPRs, the rms pressure levels are almost identical to the case without jet up to $X/D \approx 0.45$. The jet influence is obvious only at the end of the rear-body, where the $C_{p\,\mathrm{rms}}$ coefficient is about 60% higher. As already pointed out for the blunt-based body with jet, the internal flow separation[13,14] for the lowest NPR value and the resulting shock–boundary-layer interaction still do not change the external rms pressure fluctuations.

The pressure time series provide additional information on the interaction between the separated shear layer and the jet in the $L/D = 0.6$ case (Fig. 12). The more or less periodical large fluctuations can be related to the already mentioned discrete vortices that form in the near wake. This will be discussed in the next section by considering the power density spectra. At $X/D = 0.39$, random and high-frequency perturbations are superimposed on the pressure signal when the jet is running. Hence, the interaction mechanism appears to generate small-scale turbulence, which could be related to the coherent structures in the separated shear layer. The time series at $X/D = 0.55$ demonstrate that rapid oscillations, although more regular, can also exist without the jet.

Power Density Spectra

The wall-pressure spectra are now investigated to estimate the most energetic frequencies involved in the flow unsteadiness. This analysis should help to identify some aerodynamic mechanisms responsible for the pressure fluctuations. In the following, the Strouhal number Sr_l is based either on the forebody diameter $l = D$ or the rear-body extension $l = L$. The power spectral density G is then normalized by $(lq_\infty^2)/U_\infty$ so that

$$C_{p\,\mathrm{rms}}^2 = \int_0^\infty G(Sr_l)\,\mathrm{d}(Sr_l) = \int_0^\infty Sr_l G(Sr_l)\,\mathrm{d}(\log Sr_l) \qquad (1)$$

As suggested by Owen[16] for buffet studies, spectra are plotted as $\sqrt{[Sr_l G(Sr_l)]}$ in linear/log axes.

Spectra on Base Surface

The base pressure spectra of the blunt-based body are plotted in Fig. 13 at $\varphi = 0$ and 240 deg. They are representative of the two unsteady regions identified earlier on the base. The differences in the rms levels result mainly from energy at low frequency, for example, $Sr_D \leq 0.2$. A peak centered around $Sr_D = 0.08$ is clearly visible at $\varphi = 240$ deg but is replaced by a broad peak with no definite frequencies ($Sr_D \approx 0.1$) at $\varphi = 0$ deg. However, the frequency ranges are similar in the two spectra and should be due to the same physical phenomenon but with a different intensity. Moreover, these base spectra are in good agreement with the measurements of Eldred[1] and Mabey,[2] who found a broad maximum for $Sr_D \leq 0.1$ and $Sr_D = 0.06$, respectively. With regard to the other configurations with a jet or a rear-body, the base pressure spectra exhibit the same behavior at low frequency, although with a lower intensity.

Low-frequency oscillations were observed for all of the afterbody configurations tested in this study and especially in the case $L/D = 1.2$, where a reattachment occurs. They should be attributed to a flapping motion of the shear layer. This phenomenon has been identified by a number of authors for a wide range of separated flows and is a result of a large-scale unsteadiness in the bubble. In separating and reattaching flows, including the backward-facing step[12,17] or the plate with a blunt leading edge,[18,19] the flapping motion was related to successive enlargement and shrinkage of the bubble due to an oscillation of the instantaneous reattachment point. A low-frequency unsteadiness was also observed in separated flows without reattachment, such as the wake of a disk,[5] corresponding to $Sr_D \approx 0.05$. It was attributed to a simple axisymmetric pumping of the recirculation bubble.

Spectra on Rear-Body Surface

The wall-pressure spectra for $L/D = 0.6$ and 1.2 (Figs. 14–16) suggest that several kinds of flow unsteadiness can exist in the separated region other than the low-frequency flapping motion of the shear layer.

For the short rear-body extension $L/D = 0.6$ without shear layer reattachment, the spectra in the recirculation region are dominated by a narrow peak at a nearly constant frequency $Sr_D = 0.18$ in the no-jet case. The near-wake flow is characterized by a global unsteadiness, and the periodicity is attributed to the vortex shedding of large-scale turbulent structures, as observed for several axisymmetric bluff bodies.[5,6] The present measurements suggest the existence of coherent vortices in turbulent flows at very high Reynolds numbers. Further evidence of this phenomenon will be demonstrated in the next section by the consideration of the azimuthal coherence. Notice that the same Strouhal number was found by Flodrops and Desse[9] for the blunt-based body but only in the far wake at $X/D = 12$. In the present study, the wall-pressure spectra show that for this configuration the presence of a well-defined peak is less clear than in the $L/D = 0.6$ case (Fig. 13). Two hypotheses can explain this difference between the two afterbody configurations. First is the overall level of fluctuations at the base, which is much higher in the case of the blunt-based body (Fig. 5). Hence, in this situation, the wake unsteadiness at the wall is possibly hidden by random oscillations at low frequency. The second explanation could be an influence of the protruding cylinder downstream of the base, which enhances the wake unsteadiness in the $L/D = 0.6$ case. The effect on the vortex shedding process of a splitter plate with a moderate length in the wake of a blunt body was demonstrated by Bearman[20] for two-dimensional configurations.

When a supersonic jet is running, the pressure spectra shown in Fig. 15 still exhibit a narrow peak but at a slightly higher Strouhal number $Sr_D = 0.2$. Its amplitude, however, is noticeably weaker than for the no-jet case. This may be because the jet is located on the wake center and then obstructs the development of large-scale vortices. Hence, the organization of the coherent structures is probably modified, and their predominance in the wall-pressure fluctuations is reduced. Finally, the sharp increase of the rms pressure levels at the end of the rear-body earlier reported (Fig. 11) appears to result mainly from broadband energy at frequencies higher than the one associated with the large-scale vortices in the wake. These oscillations

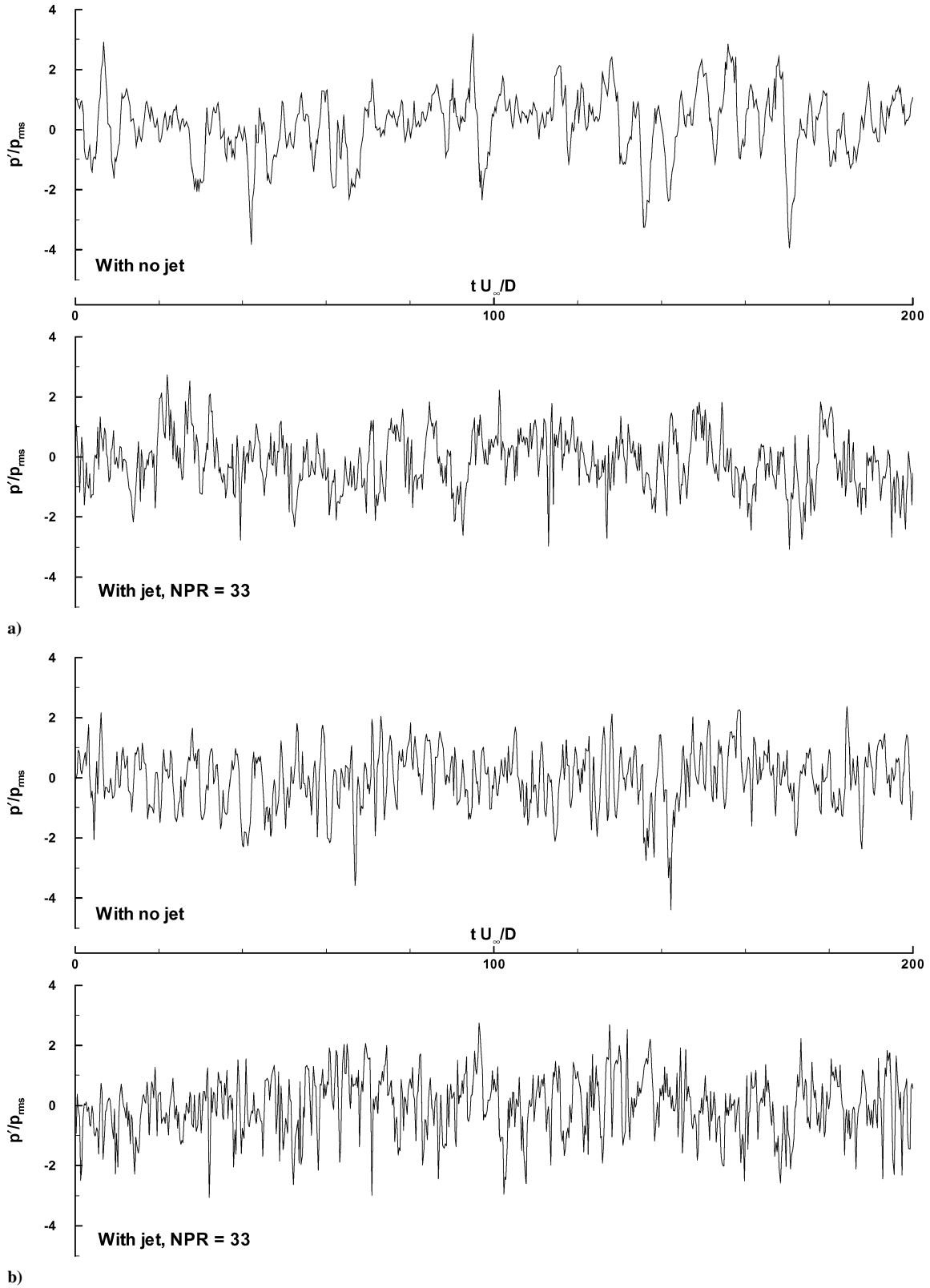

Fig. 12 Sample time series of pressure fluctuations $L/D = 0.6$ case at $X/D =$ a) 0.39 and b) 0.55.

have been attributed to the interaction between the separated shear layer and the jet located downstream of the rear-body.

For the long rear-body extension $L/D = 1.2$ (Fig. 16), the flow reattaches at the end of the rear-body. As suggested by Mabey,[11] in such situations the Strouhal number based on the reattachment length, that is, approximately L, is used. The pressure spectra exhibit different predominant frequencies, depending on the streamwise position in the recirculating bubble. Close to separation, the flow is dominated by the flapping of the shear layer, which corresponds to $Sr_L \approx 0.1$. Farther downstream, the contribution of higher frequency components becomes progressively predominant. At the end of the rear-body, a weakly defined maximum around $Sr_L \approx 0.6$ can be seen in the spectra. This frequency, which is five or six times greater than the one associated with the flapping motion of the shear layer, has been found in a wide range of separated flows with reattachment[11] and was related by several authors[18,19] to the shedding of shear layer

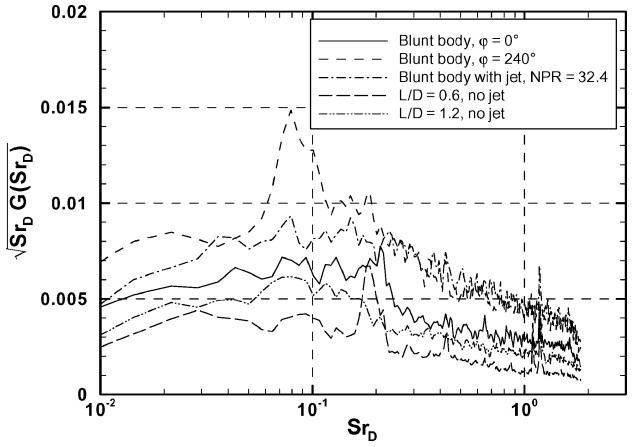

Fig. 13 Base pressure spectra at $r/R = 0.7$.

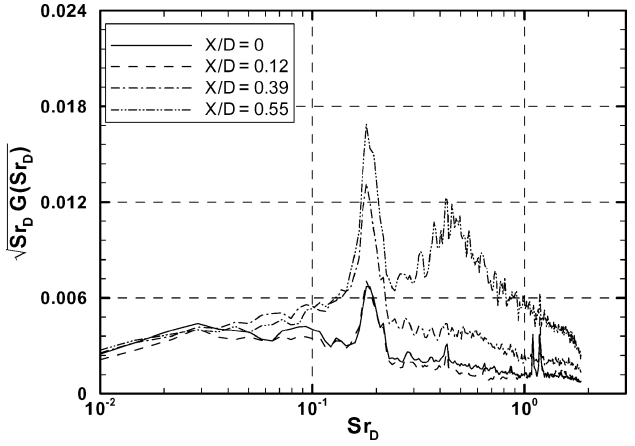

Fig. 14 Pressure spectra on rear-body for $L/D = 0.6$ with no jet.

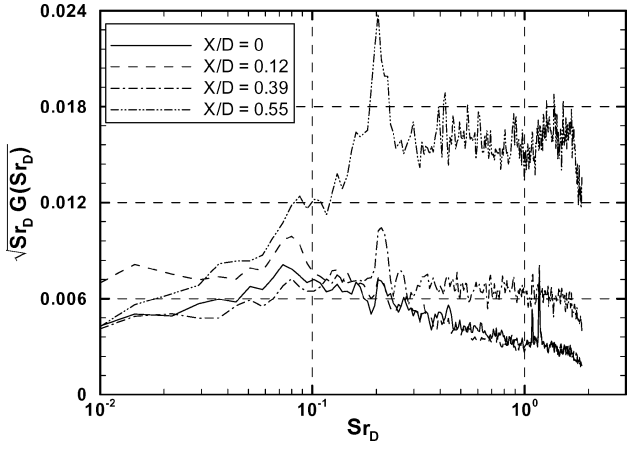

Fig. 15 Pressure spectra on rear-body for $L/D = 0.6$ with jet, NPR = 33.

vortical structures from the recirculation region in the reattachment zone. In the second-half of the external rear-body surface, and especially at $X/D = 0.72$ where the reattachment process has not yet begun, the spectra exhibit a peak centered around $Sr_L \approx 0.2$. This frequency can be related to the coherent structures in the near wake as already pointed out for the $L/D = 0.6$ case. However, for the long rear-body extension, this unsteadiness is of weaker intensity with a less definite frequency. This should be related the reattachment of the shear layer, which tends to prevent the formation of large-scale vortices in the near wake.

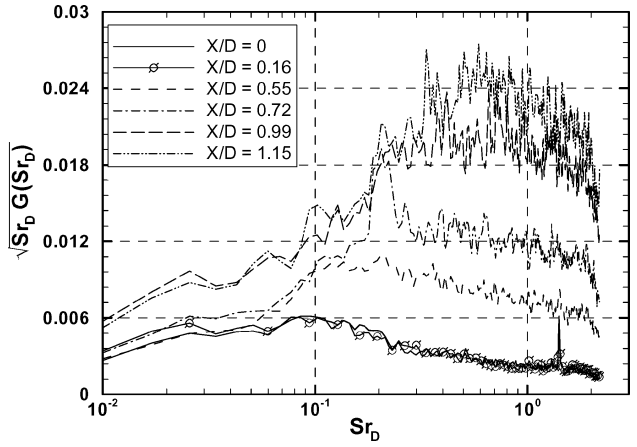

Fig. 16 Pressure spectra on rear-body for $L/D = 1.2$ with no jet.

Azimuthal Coherence

Emphasis is now placed on the spatial organization of the flow using a two-point correlation analysis. More precisely, the azimuthal coherence is investigated in the afterbody configurations where the wall pressure is influenced by the vortex shedding of large-scale structures in the near wake. Consider the random signals $p_1(r, X, \varphi_1, t)$ and $p_2(r, X, \varphi_2, t)$ obtained from two pressure transducers, located in a normal plane to the inflow. The complex coherence function may be defined as

$$C = \frac{S_{12}(r, X, \varphi_1, \Delta\varphi, f)}{\sqrt{G_1(r, X, \varphi_1, f)\, G_2(r, X, \varphi_2, f)}} = C_r + iC_i \qquad (2)$$

where S_{12} is the cross-spectral density, $\Delta\varphi = \varphi_2 - \varphi_1$. Note that $|C|$ is the classical coherence function γ.

The hypothesis of a strictly axisymmetric flow in a time-averaged sense allows two assumptions to be made regarding the cross-spectral density properties, as pointed out by Michalke and Fuchs.[21]

The first assumption is homogeneity. There should not be any preferred angle of reference φ_1:

$$S_{12} = S_{12}(r, X, \Delta\varphi, f) \qquad (3)$$

The second assumption is isotropy. When it is assumed that there is no mean swirl, the disturbances should no exhibit any particular direction of propagation:

$$S_{12}(-\Delta\varphi) = S_{12}(\Delta\varphi) \qquad (4)$$

With regard to the coherence function, the isotropy condition (4) implies that

$$C_i = 0 \Leftrightarrow \Phi = 0(\pi) \qquad (5)$$

where Φ is the coherence phase angle. Finally, the 2π periodicity of the C_r function with respect to $\Delta\varphi$ allows a Fourier decomposition in azimuthal modes:

$$C_r(\Delta\varphi, f) = \sum_{m=0}^{\infty} C_{r,m}(f) \cos(m\Delta\varphi) \qquad (6)$$

The $C_{r,m}$ coefficients can be seen as the percentage of the fluctuating energy relative to the azimuthal constituent m at a given frequency.

Practically, several rings of pressure taps nonuniformly distributed were installed at different streamwise positions on the models. A high number of transducer distances $\Delta\varphi$ could be obtained by varying the reference transducer located at angle φ_1.

The formalism described earlier is now applied to the present measurements in the $L/D = 0.6$ case without jet, where the unsteadiness associated with the coherent structures in the wake is the most obvious. The flow axisymmetry of this afterbody configuration has already been suggested by single-point measurements with

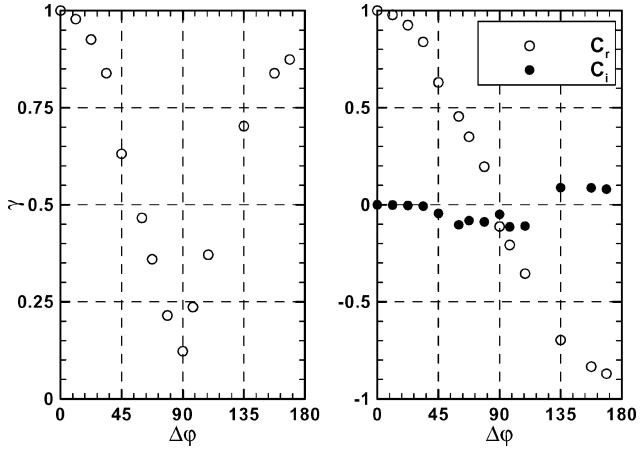

Fig. 17 Circumferential coherence distribution at the vortex shedding frequency, *X/D* = 0.55 (*L/D* = 0.6, no jet).

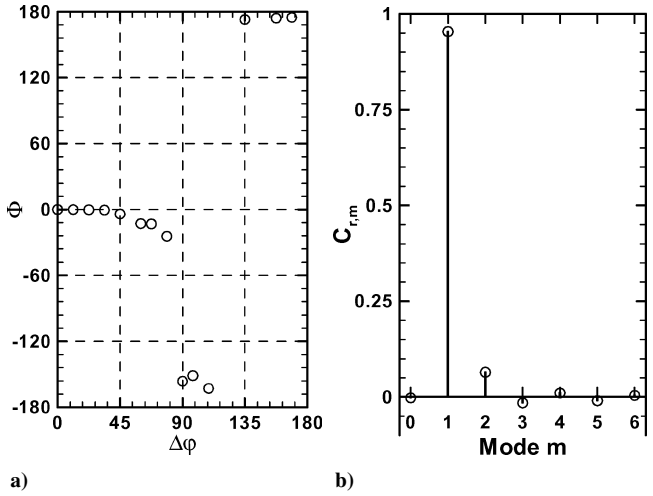

Fig. 18 Vortex shedding frequency, *X/D* = 0.55 (*L/D* = 0.6, no jet): a) phase angle Φ and b) Fourier coefficients $C_{r,m}$.

the nearly uniform circumferential distribution of the rms pressure levels as shown in Fig. 5 (opposite that of the blunt-based body case).

The $\gamma(\Delta\varphi)$ curve at the vortex shedding frequency shown in Fig. 17 exhibits a particular behavior. A classical turbulent flowfield would normally result in a monotonous decrease in the coherence with the distance between the two transducers. In the present situation, the coherence is very low for $\Delta\varphi = 90$ deg but reaches a local maximum $\gamma \approx 0.90$ for $\Delta\varphi = 180$ deg. Similar quantitative results have also been obtained on the afterbody at $X/D = 0$ and 0.12.

The flow is not exactly axisymmetric, as shown in Fig. 17, with the $C_i(\Delta\varphi)$ distribution where some scattering, although limited, around the $C_i = 0$ value is observed. The Fourier decomposition of the C_r function (Fig. 18) exhibits a strong dominance of the first azimuthal mode $m = 1$, which is associated with an antiphase relationship of the signals for $\Delta\varphi = 180$ deg. More than 90% of the pressure fluctuations at the vortex shedding frequency are due to this antisymmetric mode, the other azimuthal constituents being of negligible importance. The highly coherent pressure field for large transducer distances clearly indicates the presence of large-scale structures in the near wake. These properties of the turbulent fluctuations have ever been reported for bluff bodies,[5,6] but for probes located farther downstream in the wake. Flow visualizations[5] showed that the predominance of the $m = 1$ mode could be related to helical vortex structures randomly oriented in φ. The occurrence of highly coherent antisymmetric fluctuations on the afterbody surface should be of particular importance for further consideration of the buffet problem. Indeed, the side loads exerted on the body that can be obtained

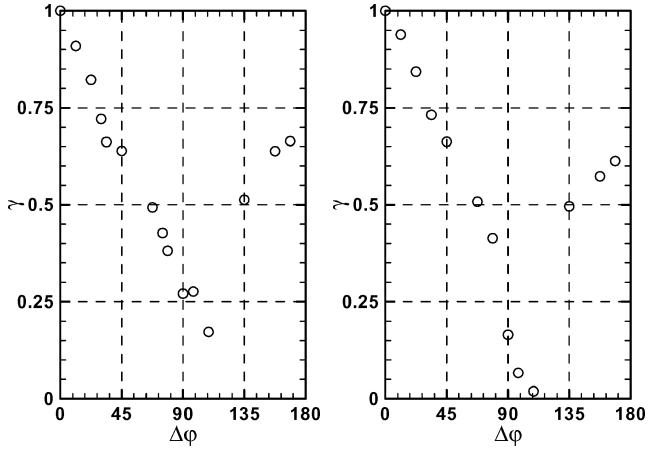

Fig. 19 Circumferential coherence distribution at the vortex shedding frequency for a) *L/D* = 0.6 with jet (NPR = 33), *X/D* = 0.55, and b) *L/D* = 1.2 without jet, *X/D* = 0.72.

by a circumferential integration of the instantaneous wall-pressure field only result from the $m = 1$ mode.

For the other afterbody configurations, such as the $L/D = 0.6$ configuration with a jet and the long rear-body extension, $L/D = 1.2$, the particular azimuthal correlation of the wall fluctuations at the vortex shedding frequency still exists, although more weakly defined, as shown in Fig. 19. The minimum of the $\gamma(\Delta\varphi)$ function is not precisely localized, but the level for $\Delta\varphi = 180$ deg remains higher than 0.5. Consequently, in these cases, the first azimuthal mode and the related helical wake structure are not as dominant as in the no-jet case for $L/D = 0.6$. This result suggests some less organized and more random large-scale structures, probably due to the small-scale turbulence generated by the separated shear layer interaction with the jet or the reattachment process on the protruding rear-body.

Conclusions

Experiments have been carried out to investigate the mean and unsteady surface-pressure field on afterbodies of revolution at high subsonic speeds. Two parameters have been tested, the extension from the base center of a cylindrical rear-body (representative of a propulsive nozzle) and the presence of a supersonic jet. It turns out that the geometric ratio L/D plays a key role in the mean and unsteady flow features.

For $L/D = 0.6$, there is no reattachment of the shear layer on the downstream surface. The wall-pressure fluctuations are affected by the formation of large-scale vortices in the wake at a frequency $Sr_D \approx 0.2$. The jet directly interacts with the recirculation bubble, which results in higher rms pressure levels on the rear-body. Although the jet constitutes an obstacle in the afterbody wake, the formation of large-scale vortices is still persistent.

For $L/D = 1.2$, the shear layer reattaches near the end of the protruding wall, where the rms pressure fluctuations are maximum. The predominant oscillations at $Sr_L \approx 0.6$ are related to the convection of turbulent eddies in the separated shear layer. The jet, which is located downstream of the recirculation bubble, has little effect on both the mean and the unsteady pressures. Finally, although less clearly dominant in the spectra, the same narrow peak at $Sr_D \approx 0.2$ as in the $L/D = 0.6$ case still exists. This shows that the flow reattachment does not totally inhibit the formation of large-scale vortex structures in the wake.

The large-scale flow phenomena have been revealed by a two-point correlation analysis. In the $L/D = 0.6$ case without jet, the instantaneous pressure field at the vortex shedding frequency is strongly dominated by the antisymmetric mode $m = 1$, although the flow is axisymmetric in a time-averaged sense. The presence of a jet or a long protruding cylinder reduces the predominance of the first mode. Note that previous flow visualizations behind bluff bodies[5,8]

suggested that the coherent vortex structures are helical. As a consequence, their development is not impossible with an obstacle, such as a jet or a long protruding cylinder, located on the wake axis.

Acknowledgments

The authors thank the Centre National d'Etudes Spatiales (CNES) (the French Space Agency) for financial support within the framework of the CNES/ONERA research and technology program Aerodynamics of Nozzles and Afterbodies. The Ph.D. Dissertation of D. Deprés was funded by CNES and ONERA.

References

[1]Eldred, K. M., "Base Pressure Fluctuations," *Journal of the Acoustical Society of America*, Vol. 33, No. 1, 1961, pp. 59–63.

[2]Mabey, D. G., "Some Measurements of Base Pressure Fluctuations at Subsonic and Supersonic Speeds," Aeronautical Research Council, ARC-CP-1204, 1972; also Royal Aircraft Establishment, RAE-TR-70148, Bedford, England, U.K., Aug. 1970.

[3]Merz, R. A., "Subsonic Base Pressure Fluctuations," *AIAA Journal*, Vol. 17, No. 4, 1979, pp. 436–438.

[4]Délery, J., and Sirieix, M., "Base Flows Behind Missiles," AGARD, Rept. LS-98, March 1979.

[5]Berger, E., Scholz, D., and Schumm, M., "Coherent Vortex Structures in the Wake of a Sphere and a Circular Disk at Rest and Under Forced Vibrations," *Journal of Fluids and Structures*, Vol. 4, 1990, pp. 231–257.

[6]Fuchs, H. V., Mercker, E., and Michel, U., "Large-Scale Coherent Structures in the Wake of Axisymmetric Bodies," *Journal of Fluid Mechanics*, Vol. 93, Pt. 1, 1979, pp. 185–207.

[7]Achenbach, E., "Vortex Shedding from Sphere," *Journal of Fluid Mechanics*, Vol. 62, Pt. 2, 1974, pp. 209–221.

[8]Taneda, S., "Visual Observations of the Flow Past a Sphere at Reynolds Numbers Between 10^4 and 10^6," *Journal of Fluid Mechanics*, Vol. 85, Pt. 1, 1978, pp. 187–192.

[9]Flodrops, J. P., and Desse, J. M., "Sillage d'un Culot Axisymétrique," Inst. de Mécanique des Fluides de Lille, Rept. IMFL-85/19, Lille, France, April 1985.

[10]Calvert, J. R., "Experiments on the Low-Speed Flow past Cones," *Journal of Fluid Mechanics*, Vol. 27, Pt. 2, 1967, pp. 273–289.

[11]Mabey, D. G., "Pressure Fluctuations Caused by Separated Bubble Flows at Subsonic Speeds," Royal Aircraft Establishment, RAE-TR-71160, Bedford, England, U.K., Dec. 1971.

[12]Driver, D. M., Seegmiller, H. L., and Marvin, J., "Time-Dependent Behavior of a Reattaching Shear Layer," *AIAA Journal*, Vol. 25, No. 7, 1987, pp. 914–919.

[13]Reijasse, P., Morzenski, L., Blacodon, D., and Birkemeyer, J., "Flow Separation Experimental Analysis in Overexpanded Subscale Rocket-Nozzles," AIAA Paper 2001-3556, July 2001.

[14]Hagemann, M., Terhardt, M., Frey, M., Reijasse, P., Onofri, M., Nasuti, F., and Ostlund, J., "Flow Separation and Side-Loads in Rocket Nozzles," *4th International Symposium on Liquid Space Propulsion*, Deutschen Zentrum für Luft- und Raumfahrt, Lampoldshausen, Germany, 2000.

[15]Maury, B., "Sondage de l'Écoulement dans la Zone Décollée en Aval d'une Marche Annulaire," ONERA, Rept. ONERA-PV-2/0334-AY, Meudon, France, June 1975.

[16]Owen, T. B., "Techniques of Pressure-Fluctuations Measurements Employed in the RAE Low-Speed Wind-Tunnels," AGARD, Rept. 172, 1958.

[17]Eaton, J. K., and Johnston, J. P., "Low Frequency Unsteadiness of a Reattaching Turbulent Shear Layer," *Turbulent Shear Flows 3*, edited by L. J. S. Bradbury, F. Durst, B. E. Launder, F. W. Schmidt, and J. H. Whitelaw, Springer-Verlag, Berlin, 1982, pp. 162–170.

[18]Kiya, M., and Sasaki, K., "Structure of a Turbulent Separation Bubble," *Journal of Fluid Mechanics*, Vol. 137, 1983, pp. 83–113.

[19]Cherry, N. J., Hillier, R., and Latour, M. E. M. P., "Unsteady Measurements in a Separated and Reattaching Flow," *Journal of Fluid Mechanics*, Vol. 144, 1984, pp. 13–46.

[20]Bearman, P. W., "Investigation of the Flow Behind a Two-Dimensional Blunt Trailing Edge and Fitted with Splitter Plates," *Journal of Fluid Mechanics*, Vol. 21, Pt. 2, 1965, pp. 241–255.

[21]Michalke, A., and Fuchs, H. V., "On Turbulence and Noise of an Axisymmetric Shear Flow," *Journal of Fluid Mechanics*, Vol. 70, Pt. 1, 1975, pp. 179–205.

R. So
Associate Editor